Dynamic Grasping in Space using Adhesive Grippers and Model Predictive Control

Roshena MacPherson, Andrew Bylard, Benjamin Hockman,
Matthew A. Estrada, Mark R. Cutkosky, Marco Pavone

***Abstract*— Spacecraft equipped with gecko-inspired dry adhesive grippers can dynamically perch on and grasp a wide variety of featureless surfaces. In this paper we explore the use of model predictive control (MPC) for autonomous docking onto and acquisition of free-floating, *spinning* objects. First, we extend previous work characterizing the dynamic grasping capabilities of these grippers to the case where both object and spacecraft are free-floating and comparably sized. We then formulate the acquisition problem as an MPC problem, whereby the terminal constraints for grasping are cast as linear constraints and the problem is solved as a Quadratic Program (thus amenable to real-time implementation on space-qualified hardware). We provide formal performance guarantees in terms of persistent feasibility and closed-loop stability, and present numerical experiments corroborating our theoretical findings.**

I. Introduction

Recently, in an effort to alleviate some of the tasks performed by astronauts, there has been increased interest in the use of small assistive free-flying robots (AFF) for grasping and manipulating objects inside and outside spacecraft. One such example is the Smart SPHERES teleoperated test bed, which was developed to perform various intra-vehicular activities aboard the International Space Station (e.g., camera work and environmental monitoring), as well as to serve as a robotics research platform in space [1]. Enabling AFFs to autonomously grasp and manipulate objects has the potential to make several human operations more safe and efficient by reducing their time spent on EVAs and performing repetitive tasks (see Fig. 1). This technology may also enable a wide range of tasks that are precluded to astronauts, such as the assembly of large-scale space structures or removal of space debris [2].

Traditionally, most grasping devices, especially in space, have relied on robotic hands that compress a target's opposing faces or grapple around its features to secure it. The precision of this operation typically requires that the target be stationary relative to the gripper for successful acquisition. In [3], the authors assume the target object has a grappling fixture and plan the spacecraft's trajectory such that its end effector reaches zero velocity relative to the grappling fixture. The grasping mechanism in [4] also grapples around various features on the target object, and relies on pinching friction forces to secure the target.

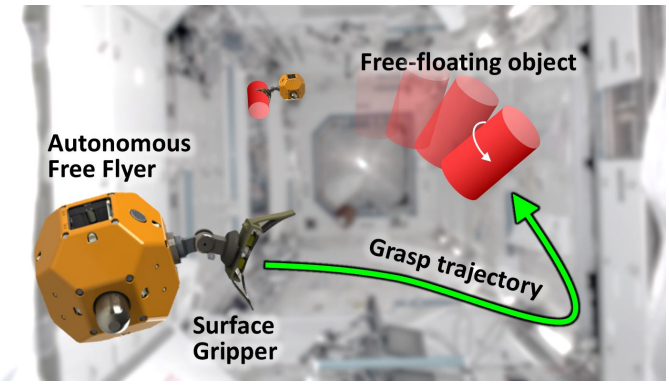

Fig. 1: Autonomous free flying spacecraft equipped with dry adhesion surface grippers may assist astronauts by grasping and manipulating objects. This paper investigates the use of MPC for autonomous perching and acquisition of free-floating, spinning objects.

Grippers that utilize surface adhesion represent a promising alternative. Inspired by the adhesive properties of geckos' feet, several grippers have been designed with a special gecko-like material that can adhere to any smooth surface, be it curved or flat [6], [7]. A useful property of these dry adhesive grippers is that, when paired with a compliant wrist mechanism, they can engage objects with non-zero relative velocity—a key advantage for acquiring drifting objects in space [9]. Previous work by the authors investigated the performance of one such gripper designed to grasp a translating and rotating object [7] (see Fig. 2). By fixing the gripper to the inertial frame, it was able to passively catch a cylindrical object thrown at it from various angles and speeds. Most importantly, dry adhesive grippers do not rely on affixing to hand-sized features, and thus can attach to a wider range of potential objects *simply by touching them*. This eliminates the need to deliberately coordinate finger contact forces, allowing the grasping task to be simplified to a rendezvous and docking problem—a well-studied problem with a rich body of literature. The controller developed in this paper will leverage much of this work.

Specifically, in this paper we investigate a Model Predictive Control (MPC) approach [19] for the task of autonomous rendezvous and docking with AFFs, which entails attaching to a free-flying object while minimizing fuel expenditure and obeying various pointwise-in-time and terminal constraints on the state and control variables (stemming, e.g., from

Roshena MacPherson, Benjamin Hockman, Matthew A. Estrada, and Mark R. Cutkosky are with the Department of Mechanical Engineering, Stanford University, CA 94305. Andrew Bylard and Marco Pavone are with the Department of Aeronautics and Astronautics, Stanford University, CA 94305. Emails: {roshenam, bylard, bhockman, estrada1, cutkosky, pavone}@stanford.edu. This work was supported by NASA under the Space Technology Research Grants Program, Grant NNX12AQ43G, and Early State Innovations Grant NNX16AD19G.

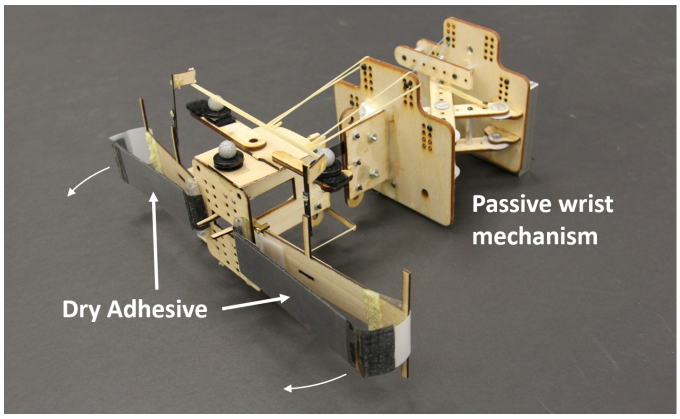

Fig. 2: Dry adhesive gripper attached to a compliant wrist mechanism used for experiments

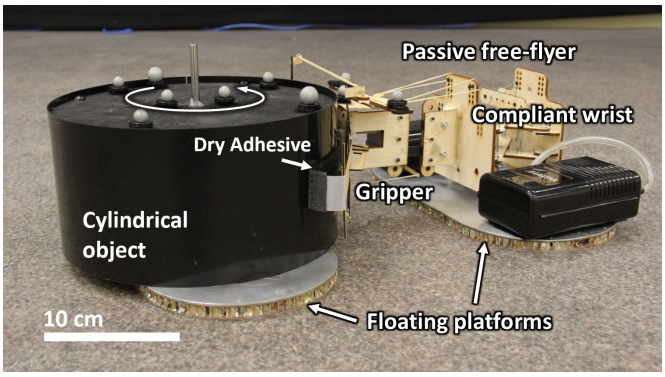

Fig. 3: Grasping experiment on the Stanford free-flyer test bed. A cylindrical object mounted on an air-bearing platform collides and attaches to another free floating platform equipped with a curved surface gripper.

physical constrains such as thrust limits and avoiding plume impingement). MPC is well-poised to tackle this problem as it provides provable performance bounds and it often leads to control architectures amenable to real-time implementation. Previous studies of MPC applied to spacecraft rendezvous and docking include [10], which treats some of the constraints as soft penalties in the cost function. This allows the problem to be formulated as a Quadratic Program (QP), thus enabling real-time implementation. Similarly, [11] restricts each phase of the problem (long range rendezvous, short range docking, etc.) to be formulated as either a Linear Program (LP) or a QP for fast online execution. In [13], the authors applied MPC to the rendezvous and docking of a spacecraft with a non-rotating platform in circular orbit around the Earth. They extended this work in [14] to the case of a rotating/tumbling object and impose state constraints to avoid debris.

Leveraging the aforementioned line of work on spacecraft rendezvous and docking, the goal of this paper is to apply MPC to the problem of autonomous perching and object acquisition with AFFs equipped with gecko-inspired grippers. Specifically, the contribution of this paper is threefold. First, in Section II, we extend our previous work in [7] on characterizing the dynamic grasping range of a curved surface gripper to the case where both spacecraft and object are free floating and in relative motion—a necessary step toward representing the terminal landing envelope (i.e., the unique terminal constraints characterizing this problem) for the MPC controller. Second, we formulate the problem of grasping spinning, featureless objects as a docking problem using MPC, and discuss correctness guarantees and its implementation as a QP (Section III). Finally, we validate the controller through a range of numerical experiments (Section IV).

II. Characterizing grasping envelope

In order to leverage the dynamic grasping capabilities of adhesive grippers for trajectory optimization, one must first understand the set of contact states for which grasping is possible, henceforth referred to as the "grasping envelope." However, the complexity of the gripper design and the highly nonlinear behavior of the dry adhesives pose a challenge for characterizing this envelope analytically. In previous work, Estrada et al. [7] experimentally characterized this envelope for a *fixed* gripper, whereby a smooth cylindrical object floating on frictionless air bearings was launched towards the gripper over a range of contact states. As the gripper is fixed, the results are only informative for the case where the spacecraft is much more massive than the object. For small AFFs, this likely will not be representative of the usual operating regime. Accordingly, our first step is to extend those results to the more general case where both object and spacecraft are floating and of comparable mass—a case in which the movement of the spacecraft itself may alter the grasping envelope.

All experiments were conducted on the Stanford free-flyer test bed—a 3x4 m granite table precisely calibrated to be flat and level—on which robotic platforms can float using frictionless air bearings, simulating a 2D microgravity environment (See Fig. 3). In nearly the exact same setup as in [7], a smooth cylindrical object (1.6 kg, 11 cm radius) is fixed to a floating platform such that it can be spun and launched towards a gripper, this time however, also mounted on a floating platform. An OptiTrack motion capture system is used to measure the trajectories of the target object, the gripper, and the free-flyer to sub-millimeter precision at 120 Hz.

The contact state between the gripper and object can be uniquely described by four parameters (in the gripper's frame), namely: relative velocity, both linear (v) and angular (Ω), angle of attack (ϕ), and lateral offset (d) (see Fig. 4). For imposing terminal velocity constraints in the MPC problem, it is most important to characterize the relationship between speed and angle of attack, which can then be translated into normal and lateral velocity constraints. In other words, by varying v and ϕ and holding d and Ω constant (both zero), and observing successful and unsuccessful grasps, one can experimentally construct a 2D slice within the 4D grasping envelope.

About fifty trials were run varying the object's speed and angle of attack for each of two scenarios: one with a high

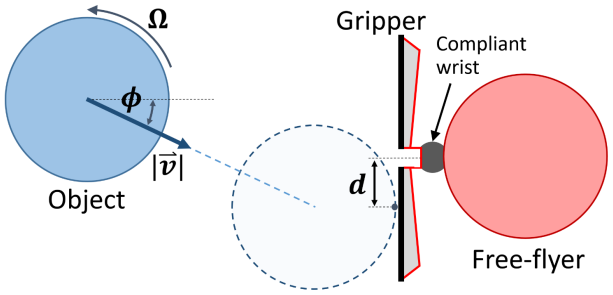

Fig. 4: The contact state between the object and free-flyer is parameterized with four variables as show in this top-down view: speed (v), angular velocity (Ω), angle of attack (ϕ), and offset (d).

mass free-flyer (4.2 kg or roughly 3 times the mass of the object), and one with a low mass free-flyer (1.7 kg or roughly the same mass as the object). The results in Fig. 5 show the data for both of these scenarios (top) compared with data for a fixed gripper from [7] (bottom). Two analytical bounds were proposed in [7] to segment the successful and unsuccessful grasps and correlate to the two dominant failure modes: (A) a minimum normal impulse that is required to depress the gripper's passive trigger mechanism, and (B) a maximum angular impulse that the gripper's compliant wrist can absorb after attaching. These bounds are still good predictors of failure for a floating free-flyer, however the normal and angular impulse must now also account for the movement of the free-flyer after collision. Thus, as the mass of the free-flyer is reduced, the minimum speed for the object to passively engage the gripper increases, the tolerable angular momentum of the object decreases, and overall, the grasping envelop shrinks.

An additional difference with respect to the case of a fixed gripper is that a third failure mode arises for high-speed collisions, whereby the floating free-flyer is pushed back by the impact before the gripper can fully close around the object.This phenomenon involves the mechanical response of gripper's compliant mount and the response time of the bistable mechanism. In [16], Yoshida discusses the contact dynamics between a robotic arm and a floating satellite in the context of impedance control and shows that appropriate impedance *matching* can mitigate the chances of pushing an object away before it is grasped by an end effector. Future work will consider similar methods of impedance matching using tunable wrist compliance [8] to reduce such a rebound effect, but for the MPC formulation presented here, we will simply enforce a constraint on the maximum velocity magnitude.

In the next section we will use the grasping envelope empirically estimated in this section to set up the MPC control problem.

III. Autonomous Grasping

In this section we formally state the control problem we wish to address, devise an MPC formulation for its solution, and discuss correctness guarantees and implementation details. We highlight that our problem formulation and tests are limited to a 2D setup; the generalization to the 3D case is

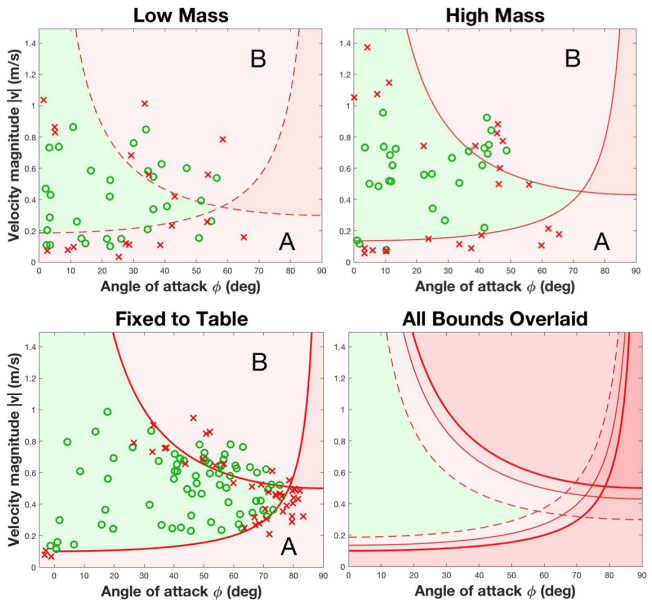

Fig. 5: Grasping envelops relating speed (v) and angle of attack (ϕ) for a non-spinning object contacting the gripper with zero offset (d). The top left, top right, and bottom left plots show show data collected for a light (1.7 kg), heavy (4.2 kg), and fixed free-flyer, respectively. The green circles and red x's depict successful and unsuccessful trials, respectively. The bottom right figure overlays the approximate envelope bounds for each of the three cases, indicating tighter bounds for lighter free-flyers.

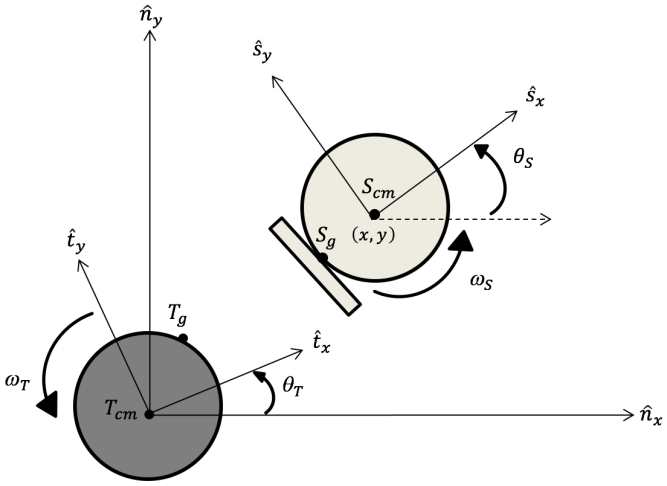

Fig. 6: Position and orientation variables of T and S as well as rotating frames t and s are depicted in the inertial frame n.

possible and will be addressed in future work. Furthermore, the underlying assumptions behind our problem formulation are that (1) the environment is obstacle-free, and (2) orbital dynamics can be ignored. Both assumptions are justified in that this paper is only concerned with the final docking phase, where obstacles have already been negotiated and orbital effects can be ignored due to the short period. In practice, in an approach phase, one would use a kinodynamic motion planner (e.g., [15]) to place the spacecraft in an obstacle-free location in the "vicinity" of the target; the MPC approach presented in this paper would then be used for the final

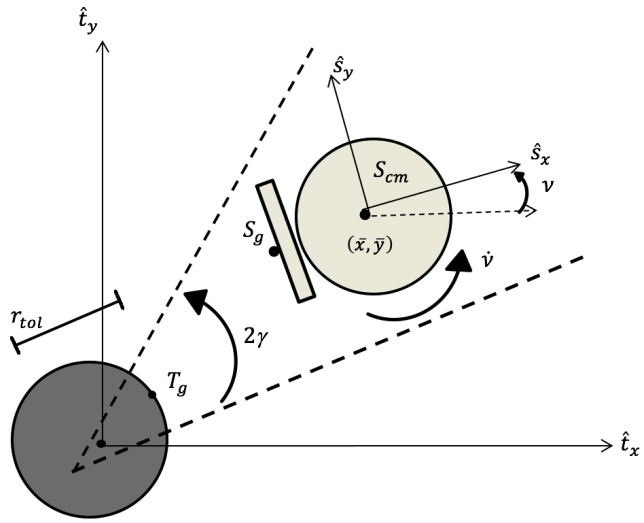

Fig. 7: The LOS cone and its defining parameters, γ and $r_{\rm tol}$ are depicted in the rotating frame t. The center line of the cone is fixed at 45° to linearize the velocity constraints

perching and grasping phase.

A. System Dynamics

We consider an autonomous docking between a target object and a spacecraft equipped with a dry adhesive gripper, denoted as T and S, respectively. The target object has a circular shape of radius r_T, mass m_T, and rotates with constant angular velocity $\omega_{\rm T}$. The spacecraft has a circular shape of radius r_S, mass m_S, moment of inertia I_{zz} in the $\hat{s_z}$ direction, and rotates with angular velocity $\omega_S(t)$. We consider a 2D problem confined to the X, Y plane. We define a point $\rm S_g$ on the surface of S at the contact point between the center of the gripper and the spacecraft body, and a point $\rm T_g$ on the surface of T that represents the target point for contact (e.g., a part of the target surface that is particularly suitable for grasping). Right-handed orthogonal bases, n, t, and s are fixed in the inertial frame, target object, and spacecraft, respectively. Defining a vector $\hat{t}_g$ that points from the target's center of mass $\rm T_{cm}$ to $\rm T_g$, basis t is defined such that the angle from $\hat{t}_x$ to $\hat{t}_g$ is $\pi/4$ for reasons that will be clear later. Angle θ_S is the angle from $\hat{n}_x$ to $\hat{s}_x$ with positive $\hat{n}_z$ sense. Angle θ_T is the angle from $\hat{n}_x$ to $\hat{t}_x$ with positive $\hat{t}_z$ sense, and $\dot{\theta}_T = \omega_T$. We define x and y as the $\hat{n}_x$ and $\hat{n}_y$ components of the position vector from $\rm T_{cm}$ to $\rm S_{cm}$. The notation is summarized in Figure 6.

Ignoring orbital dynamics effects, the dynamical equations of the spacecraft are those of a double-integrator:

$$\ddot{x} = u_x, \qquad \ddot{y} = u_y, \qquad \ddot{\theta}_S = u_\theta, \tag{1}$$

where u_x and u_y represent the independent translational control inputs (actuated, e.g., via thrusters), and u_θ represents the independent angular control input (actuated, e.g., via a reaction wheel)[1].

[1]Couplings among inputs could also be handled in our framework, as long as they can be represented (or approximated) as convex constraints.

For handling various constraints (Sect. III-B), it will be more convenient to consider the *relative* dynamics between the spacecraft and the target in a rotated, non-inertial frame fixed to T. In this rotating coordinate system, let $\bar{x}$ and $\bar{y}$ be the $\hat{t}_x$ and $\hat{t}_y$ components of the position vector from $\rm T_{cm}$ to $\rm S_{cm}$, and let ν be defined as $\nu = \theta_S - \theta_T$ (where $\dot{\nu} = \omega_S - \omega_T$). Similarly, the transformed control inputs now become

$$\bar{u}_x = F_{\bar{x}}/m_S, \quad \bar{u}_y = F_{\bar{y}}/m_S, \quad \text{and} \quad u_\theta = M/I_{zz},$$

where $F_{\bar{x}}$ and $F_{\bar{y}}$ are the $\hat{t}_x$ and $\hat{t}_y$ components of the force applied to the spacecraft, and M is the torque applied to the spacecraft. The relative dynamics in this rotating frame are linear, time-invariant:

$$\dot{\bar{X}} = \bar{A}\bar{X} + \bar{B}\bar{U},$$

where

$$\bar{A} = \begin{bmatrix} 0 & 0 & 0 & 1 & 0 & 0 \\ 0 & 0 & 0 & 0 & 1 & 0 \\ 0 & 0 & 0 & 0 & 0 & 1 \\ \omega_T^2 & 0 & 0 & 0 & 2\omega_T & 0 \\ 0 & \omega_T^2 & 0 & -2\omega_T & 0 & 0 \\ 0 & 0 & 0 & 0 & 0 & 0 \end{bmatrix}, \bar{B} = \begin{bmatrix} 0 & 0 & 0 \\ 0 & 0 & 0 \\ 0 & 0 & 0 \\ 1 & 0 & 0 \\ 0 & 1 & 0 \\ 0 & 0 & 1 \end{bmatrix},$$

and

$$\bar{X} = [\bar{x}, \bar{y}, \nu, \dot{\bar{x}}, \dot{\bar{y}}, \dot{\nu}]^T, \quad \bar{U} = [\bar{u}_x, \bar{u}_y, u_\theta]^T.$$

Finally, by discretizing the dynamics, one obtains the linear, time-invariant, discrete-time system,

$$\bar{X}(k+1) = \bar{A}_d\bar{X}(k) + \bar{B}_d\bar{U}(k), \tag{2}$$

where $\bar{X}(k)$ and $\bar{U}(k)$ are the values of the state and control vectors sampled at time step k. This is the system dynamics model we will use for the synthesis of the MPC controller.

B. State and Input Constraints

The grasping problem is constrained in three fundamental ways: (1) constraints on the control input, (2) a constraint on the contact location on the surface of the rotating target, and (3) dynamic contact constraints imposed by the gripper, as characterized in [7] and Sect. II. In particular, special consideration is required for mapping the complex 4D grasping envelope to terminal state constraints amenable for MPC.

1) Input constraints: We consider upper bound constraints for the control inputs, namely,

$$\bar{u}_x(k) \le \dot{v}_{\max}, \quad \bar{u}_y(k) \le \dot{v}_{\max}, \quad u_\theta(k) \le \dot{\omega}_{\max}, \tag{3}$$

which reflect physical thrust and torque limitations—a standard formulation for spacecraft control problems.

2) Positional (LOS) constraints: Although we are not relying on features for grasping, many objects may have preferred surfaces on which to attach (e.g., from a manipulation standpoint). Thus, we formulate an LOS position constraint as a cone centered around the target point and rotating with the object—similar to the approach in [14] for grasping rotating *features*.

The cone is parametrized by r_{tol}, an offset to define the location of the cone vertex, and γ, the half-angle of the cone (See Fig. 7) The parameter r_{tol} effectively relaxes the LOS constraints in the vicinity of the target, allowing the free-flyer to contact the object within a *range* of T_g rather than a single point. The bounds of the cone can be written as constant affine constraints in the relative coordinate frame:

$$\begin{aligned}-\tan(\pi/4+\gamma)\bar{x}(k) + \bar{y}(k) + s_1(k) \\ \leq \frac{(r_T - r_{tol})}{\sqrt{2}}(1-\tan(\pi/4+\gamma)),\end{aligned}$$

$$\begin{aligned}-\tan(\pi/4-\gamma)\bar{x}(k) - \bar{y}(k) + s_2(k) \\ \leq \frac{(r_T - r_{tol})}{\sqrt{2}}(1-\tan(\pi/4-\gamma)),\end{aligned}$$

where s_1 and s_2 are slack variables added to avoid restricting the spacecraft to stay within the cone even when it is far from its target. Accordingly, the input vector ($\bar{U}(k)$) and input matrix ($\bar{B}_d$) are augmented to include the slack variables:

$$\tilde{U}(k) = [\bar{U}(k)^T,\, s_1(k),\, s_2(k)]^T, \quad \tilde{B}_d = \left[\bar{B}_d,\, 0_{6\times 2}\right].$$

The selection of the angle γ serves two purposes: (1) it geometrically constrains the range of allowable contact locations and (2) it implicitly constrains the maximum offset of the gripper upon contact (d in Fig. 4). Referring to Fig. 7, d is related to the state variable and can be expressed as,

$$d = \tan(\nu - \text{atan}(\bar{y}/\bar{x}) - \pi/4)(r_T + r_S). \tag{4}$$

The offset limitations within the grasping envelope were explored in detail in [7], and two representative "slices" relating offset and angular velocity are shown in Fig. 8. Thus, we can jointly define constraints on offset and angular velocity by inscribing a rectangular subset within the grasping envelope (e.g., the maximum volume subset). Let $d_{\max}$ denote the maximum allowable offset (in both directions, due to symmetry), that defines the bounds of this subset.

Note that in Eq. (4), the largest value that $\text{atan}(\bar{y}/\bar{x})$ can achieve within the LOS cone is γ. Thus, if the magnitude of ν can be constrained to be below a certain upper bound, say $\nu_{\max}$, then the offset is also constrained ($d \leq d_{\max}$) within the LOS cone provided that

$$\gamma \leq \nu_{\max} - \text{atan}(-d_{\max}/(r_T + r_S)) - \pi/4.$$

Unfortunately, posing a bound on ν directly is difficult. Hence, our approach is to penalize the state variable ν in the cost of the MPC problem, and backtrack an estimate of the worst-case value of ν upon collision, which is then used to fine-tune γ.

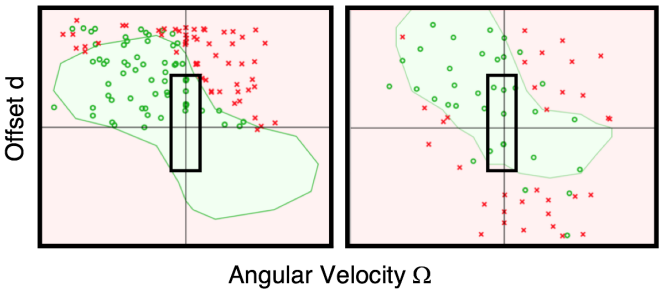

Fig. 8: Grasping envelope relating angular velocity (ω_T) and offset (d) for $\theta_T = 0$ (left plot) and $\theta_T = \pi/4$ (right plot). $||v||$ = 0.27 m/s in both cases. A conservative rectangular subset is inscribed within the grasping envelope to define the offset and angular velocity constraints for the MPC problem.

3) Angular constraints: The angle of attack ϕ is constrained to be less than $\pi/4$—the maximum angle of attack for which reliable grasping was observed. The 45° orientation of the LOS cone in the rotating frame allows this constraint to be imposed as simply a negative velocity in the $\hat{t}_x$ and $\hat{t}_y$ directions (i.e. $\dot{\bar{x}}$, and $\dot{\bar{y}} \leq 0$).

4) Translational velocity constraints: We desire to restrict the magnitude of $\bar{v}_{\text{col}}$, the velocity of S_{cm} upon collision with T. To do so without restricting the magnitude of the velocity when the spacecraft is far away, we introduce constraints on $\dot{\bar{x}}$ and $\dot{\bar{y}}$ that are a function of the one norm of the distance from T_g to S_g. Specifically, given a maximum velocity magnitude $\bar{v}_{\max}$ that the spacecraft can have upon impact, we seek to conservatively constrain the components of the velocity vector upon impact as

$$|\dot{\bar{x}}_{\text{col}}| \leq \frac{\bar{v}_{\max}}{\sqrt{2}}, \qquad |\dot{\bar{y}}_{\text{col}}| \leq \frac{\bar{v}_{\max}}{\sqrt{2}}. \tag{5}$$

Defining $\psi := |\bar{x}| + |\bar{y}|$, the velocity constraints then read as

$$|\dot{\bar{x}}| \leq \eta\psi, \qquad |\dot{\bar{y}}| \leq \eta\psi \tag{6}$$

where $\eta > 0$ is a constant that defines the shape of the feasible set and is chosen to enforce constraint (5) upon impact, without overly restricting the velocity of the spacecraft far from the target. In particular, we choose η by setting $\psi = r_T + r_S$ and $\dot{\bar{x}} = \bar{v}_{\max}/\sqrt{2}$, resulting in $\eta = \bar{v}_{\max}/(r_T + r_S)\sqrt{2}$. To linearize constraint (6), we add the auxiliary constraints

$$\bar{x} \geq 0, \qquad \bar{y} \geq 0. \tag{7}$$

Constraint (7) effectively restricts the feasible set of positions for the spacecraft (in the rotating frame) to the upper-right quadrant. On the computational side, constraint (7) allows to use convex optimization techniques for the solution to the MPC problem. On the practical side, constraint (7) has a very moderate impact on the generality of the approach as (1) it is reasonable to assume that the terminal condition for the approach phase (handled via a kinodynamic motion planner) is in the quadrant where the target point is (the upper-right quadrant, as assumed without loss of generality) to avoid excessive propellant expenditure, and (2) for practical

grippers, $\gamma \leq \pi/4$ (to avoid excessive offsets upon impact), thus the LOS cone (whose center line coincides with the $\hat{x} = \hat{y}$ line, as discussed in Section III-A) is fully contained in the upper-right quadrant.

We mention that if $\bar{v}_{\text{col}}$ has a value that is on par with the maximum velocity that can be possibly achieved by the spacecraft, then one could simply replace the velocity constraint (6) with the simpler, uniform constraint

$$|\dot{\hat{x}}| \leq \frac{\bar{v}_{\max}}{\sqrt{2}}, \qquad |\dot{\hat{y}}| \leq \frac{\bar{v}_{\max}}{\sqrt{2}}. \tag{8}$$

Finally, we also consider a minimum velocity magnitude constraint, since, as shown by region A in Figure 5, below a certain impulse the gripper's passive trigger mechanism is not engaged. Our approach is to place the equilibrium point for the MPC controller at the center of the target object rather than the target point itself, allowing the spacecraft to maintain non-zero speed upon collision with T_g. The state penalty is then tuned so that (for an exhasutive range of tests) the final velocity upon impact is consistently no smaller than 0.18 m/s.

5) Angular velocity constraints: A similar approach is used to bound ω_S upon contact with T_g. Specifically, we set the constraint

$$|\omega_S| \leq \eta_\omega \psi,$$

where $\eta_\omega > 0$ is again chosen to enforce the angular speed of the spacecraft is below the maximum angular speed for a reliable grasp, as determined from Figure 8.

C. Model Predictive Controller

We are now in a position to design the MPC controller for autonomous perching and acquisition. Specifically, we seek to drive the state of the system to the origin (corresponding to the center of the target object, as discussed in the previous section), while obeying the system dynamics described in III-A (in a rotating frame) and respecting the set of state-input constraints discussed in Section III-B.

To ensure convergence of the system to the origin, the first step is to solve the infinite-horizon unconstrained LQR problem,

$$\min_{\bar{\mathbf{U}}(\cdot)} \sum_{k=0}^{\infty} \bar{X}(k)^T Q \bar{X}(k) + \bar{U}(k)^T R \bar{U}(k) \tag{9}$$

where $\bar{\mathbf{U}}(\cdot) = \{\bar{U}(0), \bar{U}(1), ...\}$, Q is a positive definite matrix penalizing the state values, and R is a positive definite matrix penalizing the control effort. Let P be the solution to the discrete algebraic Riccati equation associated with the above problem. Following [19, Theorem 13.2], we add the value function $\bar{X}^T P \bar{X}$ to the cost function of the MPC problem to guarantee closed-loop stability. In turn, to ensure persistent feasibility (i.e., recursive feasibility of the MPC problem), we follow [19, Theorem 13.1] and the arguments in [19, pages 262-263], and compute the positively invariant set $\mathcal{X}_f$ for the closed loop system $\bar{X}(k+1) = (\bar{A}_d + \tilde{B}_d F_\infty)\bar{X}(k)$, where F_∞ is the optimal feedback controller associated with the problem in Eq. (9). We ensure persistent feasibility by enforcing that the state of the system at the last step in the MPC problem is in $\mathcal{X}_f$.

To encode state-input constraints, we define matrices

$$\bar{C} = \begin{bmatrix} -\tan(\pi/4+\gamma) & 1 & 0 & 0 & 0 & 0 \\ \tan(\pi/4-\gamma) & -1 & 0 & 0 & 0 & 0 \\ -\eta & -\eta & 0 & -1 & 0 & 0 \\ -\eta & -\eta & 0 & 1 & 0 & 0 \\ -\eta & -\eta & 0 & 0 & -1 & 0 \\ -\eta & -\eta & 0 & 0 & 1 & 0 \\ -\eta_\omega & -\eta_\omega & 0 & 0 & 0 & -1 \\ -\eta_\omega & -\eta_\omega & 0 & 0 & 0 & 1 \\ 0 & 0 & 0 & 1 & 0 & 0 \\ 0 & 0 & 0 & 0 & 1 & 0 \\ -1 & 0 & 0 & 0 & 0 & 0 \\ 0 & -1 & 0 & 0 & 0 & 0 \end{bmatrix},$$

and

$$\bar{D} = \begin{bmatrix} 0_{2\times 3} & I_{2\times 2} \\ 0_{10\times 3} & 0_{10\times 2} \end{bmatrix}.$$

These matrices are used to define an auxiliary 12-dimensional vector $\bar{Y}$ used to enforce the constraints. Explicitly, we define:

$$\bar{Y} := \bar{C}\bar{X} + \bar{D}\tilde{U},$$

where $\tilde{U}$ is the augmented control input. The constraints are then enforced as

$$\bar{Y} \leq \bar{Y}_{\max},$$

where $\bar{Y}_{\max}$ is a vector of constraint thresholds that can be readily gleaned from Section III-B.

The MPC prediction model is then

$$\begin{aligned} \bar{X}(j+1|k) &= \bar{A}_d \bar{X}(j|k) + \tilde{B}_d \tilde{U}(j|k), \\ \bar{Y}(j|k) &= \bar{C}\bar{X}(j|k) + \bar{D}\tilde{U}(j|k), \end{aligned} \tag{10}$$

where $\bar{X}(j+1|k)$ is the value of the state (in the rotating reference frame) at time $j \geq k$ predicted at time k, $\tilde{U}(j|k)$ is the value of the (augmented) input at time $j \geq k$ predicted at time k, and $Y(j|k)$ is the auxiliary 12-element vector used to enforce the state constraints. The MPC controller then solves at every time step k the optimization problem

$$\begin{aligned} \min_{\tilde{\mathbf{U}}(k)} \ & \|\bar{X}(N|k)\|_P + \sum_{j=0}^{N-1} \|\bar{X}(j|k)\|_Q + \|\tilde{U}(j|k)\|_{\bar{R}} \\ s.t. \quad & \bar{X}(j+1|k) = \bar{A}_d \bar{X}(j|k) + \tilde{B}_d \tilde{U}(j|k) \\ & C\bar{X}(j|k) + \bar{D}\tilde{U}(j|k) \leq \bar{Y}_{\max} \\ & \bar{X}(0|k) = \bar{X}(k) \\ & \tilde{U}(j|k) \leq \tilde{U}_{\max} \\ & \tilde{U}(j|k) \geq \tilde{U}_{\min} \\ & \bar{X}(N|k) \in \mathcal{X}_f \end{aligned} \tag{11}$$

where N is the prediction horizon, $\|y\|_L$ denotes $y^T L y$ for a vector y and a positive definite matrix L, $\bar{R}$ has the same entries as R plus two columns to account for the two slack variables associated with the LOS constraints, $\tilde{U}_{\max}$ and

$\tilde{U}_{\min}$ encode the input constraints (described in Section III-B), and $\mathcal{X}_f$ is the positively invariant set discussed above. The entries in $\bar{R}$ corresponding to the slack variables are weighted heavily to encourage satisfaction of the constraints. At the beginning of each control cycle, using the measured initial values of the state vector $\bar{X}(k)$, the MPC controller solves the optimization problem above for the optimal control actions $\tilde{\mathbf{U}}^*(k)$, and then applies the first element to the system, i.e., $\tilde{U}(0|k)$. Note that the MPC problem is a quadratic program, which can be quickly solved on space-qualified hardware as needed for real-time implementation.

Assuming the initial condition lies in the maximally positive invariant set $\mathcal{X}_0$ for the closed-loop system (under the MPC control law), the closed-loop system will converge to the origin [19, Theorem 13.2], which, as discussed in Section III-B, corresponds to a reliable grasp. Accordingly, the approach phase drives the state to $\mathcal{X}_0$, which can be computed numerically.

IV. Numerical Experiments

In this section we evaluate via numerical experiments the performance of the MPC algorithm presented in Section III-C. To solve Eq. (11) we used MPT3 [21], an open source, MATLAB-based toolbox for parametric optimization, computational geometry, and MPC. The size and distance parameters were set to $r_T = r_S = 0.15$ m and r_{tol} = 0.17 m. The maximum input constraints were $\dot{v}_{max} = 0.2$ ms^{-2} and $\dot{\omega}_{max} = 0.2$ s^{-2}. The penalty on the slack variables was $\rho = 10^6$, the control penalty matrix was $R = 10^2 I$, and the state penalty matrix was $Q = 10^3 I$, with relative angle penalty $Q(3,3)$ increased to 10^4. As discussed previously, the weights on ν, $\dot{\nu}$, and u_θ were tuned ensure fast convergence of ν to 0. The weight on $\bar{x}$ was tuned until no simulations resulted in contact with T_g at speeds lower than 0.18 m/s.

Figure 9 depicts an example trajectory demonstrating the use of the slack variables in the LOS cone constraints. The spacecraft is able to start far outside the cone, return to it, and successfully contacts the target point $\mathrm{T_g}$.

Figure 10 depicts the region of attraction of the controller in the non-inertial frame given $\nu_0 = \dot{\bar{x}}_0 = \dot{\bar{y}}_0 = \dot{\nu}_0 = 0$, $\gamma = 9.5°$, and ω_T = 0.035 rad/sec. At each location the MPC horizon length was varied between 10 and 30 to find the minimum horizon length to ensure feasibility. Since a smaller horizon time means fewer variables and thus faster computation times, this plot can be used to select the smallest horizon time possible while still ensuring feasibility.

V. Conclusions

In this work, we considered the steering of free-flying spacecraft to successfully grasp spinning objects using dry adhesive grippers. The grasping envelope of the gripper was further explored experimentally, examining the dynamics of two floating bodies having various masses. A subset of the grasping envelope was cast as linear constraints amenable to a QP formulation. From this, an MPC controller was designed to target a grasping region on a spinning object, demonstrating successful enforcement of all constraints.

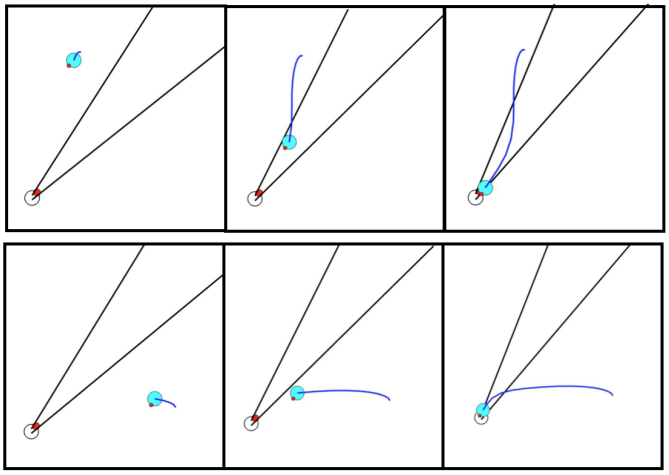

Fig. 9: Simulations showing two example trajectories and convergence of spacecraft to the LOS cone. In the top row of snapshots the cone rotates towards the spacecraft. In the bottom row of snapshots the cone rotates away from the spacecraft.

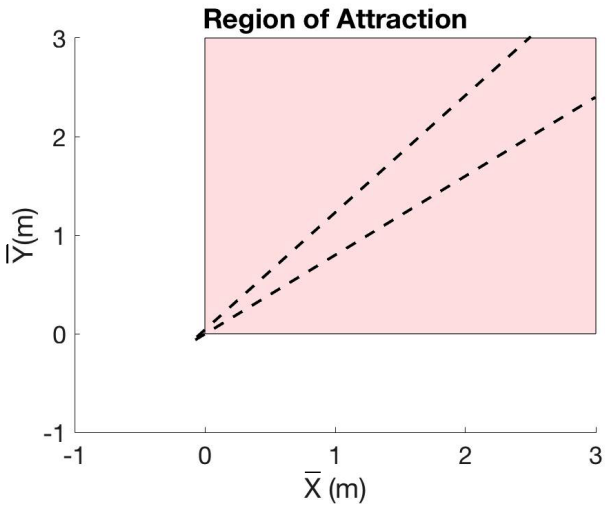

Fig. 10: Plot showing region of attraction for zero initial velocity in the non-inertial frame, $\gamma = 9.5°$, $\omega_T = 0.035$ rad/sec. Colored region is region of attraction. All points within colored region are feasible with $N \geq 12$. Dashed lines depict the LOS cone.

Further work will include validating the controller on an experimental test bed of free-flying robots. In addition, this controller can easily be extended to target any part of a spinning object, rather than restricting the goal to a particular region. Finally, a study may be warranted to explore trade-offs in adjusting the subset of the grasping envelope used to formulate controller constraints.

References

[1] T. Fong, M. Micire, T. Morse, E. Park, C. Provencher, V. To, D. W. Wheeler, D. Mittman, R. J. Torre, and E. Smith, "Smart SPHERES: A Telerobotic Free-Flyer for Intravehicular Activities in Space", Addison-Wesley, Reading, Massachusetts, 1993.

[2] National Research Council (US). Steering Committee for NASA Technology Roadmaps. "NASA Space Technology Roadmaps and Priorities: Restoring NASA's Technological Edge and Paving the Way for a New Era in Space" (Tech. Rep.). National Academies Press, 2012.

[3] F. Aghili, "A Prediction and Motion-Planning Scheme for Visually Guided Robotic Capturing of Free-Floating Tumbling Objects with Uncertain Dynamics," *IEEE Transactions on Robotics*, vol. 28, no. 3, June 2012. pp. 634-649.

[4] P. Motaghedi, "On-orbit Performance of the Orbital Express Capture System", *Proceedings of Sensors and Systems for Space Applications II, SPIE*, vol. 6958 (R. T. Howard; and P. Motaghedi, eds.) (SPIE, Bellingham WA, 2008), pp. 69580E-169580E-12.

[5] M. Henrey, J. Tellez, K. Wormnes, L. Pambaguian, C. Menon, "Sticking in Space: Manufacturing Dry Adhesives and Testing their Performance in Space Environemnts", in *12th Symp. on Adv. Space Technologies in Robotics and Automation*, 2013, Noordwijk, Netherlands.

[6] H. Jiang, E. W. Hawkes, V. Arutyunov, J. Tims, C. Fuller, J. P. King, C. Seubert, H. L. Chang, A. Parness, and M. R. Cutkosky, "Scaling Controllable Adhesives to Grapple Floating Objects in Space," in *Proc. IEEE Conf. on Robotics and Automation*, 2015.

[7] M. Estrada, B. Hockman, A. Bylard, E. Hawkes, M. Cutkosky, M. Pavone, "Free-Flyer Acquisition of Spinning Objects with Gecko-Inspired Adhesives," in *Int. Conf. Robotics and Automation*, Stockholm, 2016.

[8] M. Estrada, H. Jiang, B. Noll, E. Hawkes, M. Pavone, M. Cutkosky, "Force and Moment Constraints of a Curved Surface Gripper for Assistive Free-Flyers," in *Int. Conf. Robotics and Automation*, Singapore, 2017, submitted.

[9] E. W. Hawkes, D. L. Christensen, E. V. Eason, M. A. Estrada, M. Heverly, E. Hilgemann, H. Jiang, M. T. Pope, A. Parness, and M. R. Cutkosky, "Dynamic surface grasping with directional adhesion," in *2013 IEEE/RSJ International Conference on Intelligent Robots and Systems*, Tokyo, Japan, Nov. 2013.

[10] A. Weiss, M. Baldwin, R. Erwin, and I. Kolmanovsky, "Model Predictive Control for Spacecraft Rendezvous and Docking: Strategies for Handling Constraints and Case Studies," *IEEE Trans. Control Syst. Tech.* vol. 23, no. 4, pp. 1638-1647, 2015.

[11] E. Hartley, P. Trodden, A. Richards, and J. Maciejowski, "Model Predictive Control System Design and Implementation for Spacecraft Rendezvous," *Control Engineering Practice*, vol. 20, no. 7, pp. 695-713, 2012.

[12] L. Singh, S. Bortolami, and L. Page, "Optimal Guidance and Thruster Control in Orbital Approach and Rendezvous for Docking using Model Predictive Control," in *AIAA Guidance, Navigation, and Control Conf. and Exhibit*, Toronto, Canada, Aug. 2010.

[13] H. Park , S. Di Cairano, and I. Kolmanovsky, "Model Predictive Control of Spacecraft Docking with a Non-rotating Platform," in *IFAC 18th World Congress*, Milano, 2011, pp. 8485-8490.

[14] S. Di Cairano, H. Park, and I. Kolmanovsky, "Model Predictive Control Approach for Guidance of Spacecraft Rendezvous and Proximity Maneuvering," *Int. J. Robust Nonlinear Control*, vol. 22, no. 12, pp. 1398-1427. May, 2012.

[15] E. Schmerling, L. Janson, and M. Pavone, "Optimal Sampling-based Motion Planning under Differential Constraints: the Drift Case with Linear Affine Dynamics," in *Proc. IEEE Conf. on Decision and Control*, 2015.

[16] K. Yoshida, H. Nakanishi, N. Inaba, H. Ueno, and M. Oda, "Contact Dynamics and Control Strategy Based on Impedance Matching for Robotic Capture of a Non-cooperative Satellite," in *The 15th CISM-IFToMM Symposium on Robot Design, Dynamics, and Control - ROMANSY*, St-Hubert, Canada, 2004.

[17] M. Grant and S. Boyd. "CVX: Matlab Software for Disciplined Convex Programming, version 2.0 beta." `http://cvxr.com/cvx, September2013`.

[18] M. Grant and S. Boyd. "Graph Implementations for Nonsmooth Convex Programs, Recent Advances in Learning and Control (a tribute to M. Vidyasagar)", V. Blondel, S. Boyd, and H. Kimura, editors, pp. 95-110, Lecture Notes in *Control and Information Sciences*, Springer, 2008. `http://stanford.edu/~boyd/graph\_dcp.html`.

[19] F. Borrelli, A. Bemporad, and M. Morari, "Predictive Control for linear and hybrid systems", 2015. Available at: http://www.mpc.berkeley.edu/mpc-course-material

[20] A. Richards and J. How. "Model Predictive Control of Vehicle Maneuvers with Guaranteed Completion Time and Robust Feasibility," in *Proc. 2003 American Control Conf.*, Denver, 2003.

[21] M. Herceg, M. Kvasnica, C.N. Jones and M. Morari. "Multi-Parametric Toolbox 3.0," in *Proc. of the European Control Conference*, pp. 502-510, Zurich, Switzerland, 2013.